Korean J. Chem. Eng., 36(1), 21-29 (2019)
DOI: 10.1007/s11814-018-0165-y

pISSN: 0256-1115
eISSN: 1975-7220

Asymmetrical breakup and size distribution of droplets in a branching microfluidic T-junction

Pengcheng Ma, Taotao Fu†, Chunying Zhu, and Youguang Ma†

State Key Laboratory of Chemical Engineering, School of Chemical Engineering and Technology, Tianjin University, Tianjin 300072, P. R. China
(*Received 10 June 2018 • accepted 10 October 2018*)

Abstract−The breakup and distribution of droplets at a branching T-junction were investigated experimentally by a high-speed camera. The effects of two-phase flow rates, two-phase Reynolds number and capillary number of the dispersed phase on droplet volume distribution were studied. The results indicated that the volume distribution ratio λ decreases first and then increases with the increase of two-phase flow ratio Q_d/Q_c. Similarly, as the Reynolds number Re_c of the continuous phase increases, the volume distribution ratio λ also decreases at first and then increases. The increase of Reynolds number Re_d of the dispersed phase would lead to a reduction in the volume distribution ratio λ. Moreover, the increase of the capillary number Ca_d of dispersed phase could result in an increase in the volume distribution ratio λ. Correlations for predicting the volume distribution ratio were proposed, and the calculated results show good agreement with experimental data.

Keywords: Microchannel, Droplet, Breakup, Distribution, Interface

INTRODUCTION

Microfluidics has drawn extensive attention due to the advantages of fast heat and mass transfer rate, high safety and ease of control. Microfluidics technique could be applied to precisely control a chemical reaction, in which each droplet could be regarded as a micro-reactor to restrict effectively backmixing [1]. In addition, microfluidics technique requires fewer samples and has fast response times, and thereby it provides broad potential application in the fields of biology, medicine and chemistry [2,3]. Two-phase microfluidics technique, as an important branch of multiphase microfluidics technique, focuses mainly on droplet (bubble) formation [4,5], movement [6], breakup [7,8], distribution [9], filtering [10], and coalescence [11].

T-junction is one of the most basic elements in microfluidic devices for the breakup of droplets (bubbles), which includes two types: symmetric T-junction and asymmetric T-junction. Symmetric microfluidic T-junctions could be used to produce monodisperse daughter droplets (bubbles) [12-15]. However, if all researches are focused only on producing droplets with a single size, the merit of microfluidic production controllability will be greatly limited. Accordingly, studies for the hydrodynamics of droplets (bubbles) passing through a microfluidic asymmetric T-junction are of great significance. Generally, the volume distribution of droplets (bubbles) at the T-junction relies primarily on the different resistances in the downstream channels. The resistance in the channel mainly consists of the resistance of the continuous phase in the channel, the additional resistance from the droplets (bubbles), and the resistance stemming from the collision of droplets (bubbles) at the T-junction [9]. The different hydraulic resistances in the two downstream channels could bring about droplets (bubbles) breakup asymmetrically at asymmetric T-junction; this provides an effective and feasible approach to produce simultaneously the droplets (bubbles) with different sizes.

The asymmetric T-junction could be further divided into two types. The first type evolved from the symmetric T-junction, but there exist differences between the length or width of the two downstream channels. Link et al. [7] studied the droplet breakup at the T-junction with two downstream channels of the same cross-section but different lengths, and they found that the volume distribution ratio of two daughter droplets is inversely proportional to the ratio of the length of the two downstream channels. Bedram et al. [16] simulated the droplet breakup process at the T-junction with the two downstream channels of same the length but different widths. Subsequently, Samie et al. [17] investigated experimentally the breakup behavior of droplets at the T-junction of triangular cross-section; the two downstream channels have the same length but different widths. Both of them found that the volume ratio of two daughter droplets to the two downstream channels width ratio shows a power law relationship. Fu et al. [18] studied the bubble breakup at a T-junction with an asymmetric loop; the effect of the additional resistance due to the presence of bubbles in the downstream microchannels was taken into account, and a theoretical model for predicting bubble distribution ratio was proposed.

The second type is branching T-junction. Unlike the first type, one downstream channel of the branching T-junction is in line with the main channel, and another one is at an angle of 90 degrees to the main channel. In practical application, one stream is usually required to split into multiple streams due to regional restrictions or engineering needs, and accordingly the branching T-junction could be used as a simple distributor to achieve the distribution of

†To whom correspondence should be addressed.
E-mail: ttfu@tju.edu.cn, ygma@tju.edu.cn

streams. Wang et al. [19] investigated the transition mechanism between different flow patterns of bubbles at the branching T-junction, and found that the bubbles break up more easily at branching T-junction in comparison with that at symmetric and the first type asymmetric T-junction. Wang et al. [20] studied the interfacial dynamics of bubble breakup with permanent obstruction, and explored the influences of two-phase superficial velocity and liquid viscosity on bubble breakup. Moritani et al. [21] succeeded in generating multiple daughter droplets with high monodispersity from a mother droplet in a microfluidic system consisting of several branching T-junctions, to improve production efficiency. Chen et al. [22] investigated experimentally the distribution of gas-liquid two-phase in parallel micro-T channels, and found that bubbles could block some branches due to the high interfacial tension between pure water and nitrogen. Liu et al. [23] studied the phase distribution of gas-liquid two-phase slug flow in horizontal parallel microchannels, and found that the two-phase distribution at the parallel microchannels depended dramatically on the bubble length and the flow velocity at the inlets. In addition, they also found that the hydrodynamics in the upstream branch channels could affect the phase distribution of the adjacent downstream branch channel. Obviously, the study of droplet breakup at a single branching T-junction could provide a theoretical basis for the design and application of multi-parallel microchannel system.

The study of droplet breakup and volume distribution at the branching T-junction is of essential significance to multiphase microfluidics. Although several efforts have been devoted to droplet (bubble) breakup at asymmetric T-junctions, the study of droplet breakup at a branching microfluidic T-junction (a special asymmetric T-junction) remains still far from sufficient up to now. Therefore, the droplet breakup and volume distribution at the branching T-junction were observed and investigated experimentally by a high-speed camera in the present work. Furthermore, the influences of two-phase flow rates, two-phase Reynolds numbers and capillary numbers of the dispersed phase on droplet distribution during breakup were also studied systematically.

MATERIAL AND METHODS

The microfluidic device used in the experiments is sketched in Fig. 1. The microchannel includes a cross-focusing device to form droplets and a branching T-junction to break up the formed droplets. The continuous phase (mineral oil) was introduced from the two lateral channels at a flow rate of Q_c and the dispersed phase (glycerol-water solution) was introduced from the main channel at a flow rate of Q_d. The two immiscible flow streams encountered at the cross-focusing device, dispersed phase was pinched off by the continuous phase to form droplets. Then, the formed droplet flowed downstream and broke up into two daughter ones at the branching T-junction. The microfluidic device was fabricated in a polymethyl methacrylate (PMMA) plate (100×60×10 mm^3) and sealed by another PMMA plate with the equal size by screws. The cross section of microchannel is 400 μm (wide)×400 μm (deep).

In the experiment, an inverted microscope (ECLIPSE Ti-CU, Nikon, Japan) connected to a high-speed camera (Fastcam SA1.1, Japan) was placed above the microfluidic device to capture the

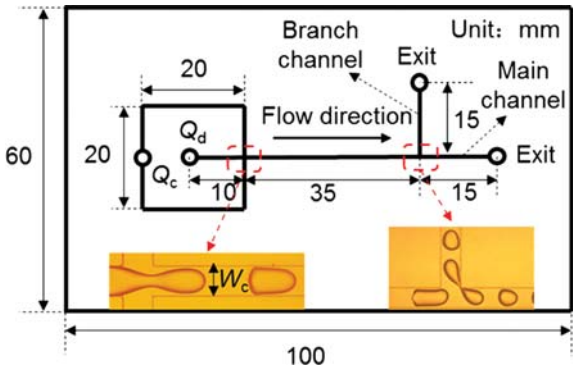

Fig. 1. Schematic diagram of the microfluidic device. Droplets are formed at the upstream cross-focusing structure and then the formed droplet breaks up into two daughter ones at the branching T-junction. The cross section of microchannel is 400 μm (wide)×400 μm (deep).

breakup process of droplets at the branching T-junction, the recording rate of the camera was 1,000 fps (frames per second). The 12 VDC halogen lamp was used to illuminate the microfluidic device, and the power was supplied by Nikon TI-PS 100 W (Japan). The system was required to reach a steady state before recording the images when the operating conditions were changed. The dispersed and continuous phases were injected into the device from syringes driven by two syringe pumps (Harvard Apparatus, PHD 22/2200, USA), respectively. In the experiment, the flow rates of the continuous phase Q_c and the dispersed phase Q_d were $0.4<Q_c<6.0$ ml/h, $1.0<Q_d<4.0$ ml/h.

Glycerol-water solution with the glycerol mass concentration of 0, 10%, 20% and 30% was used as the dispersed phase. The mineral oil with 4 wt% Span-20 was used as the continuous phase. The added Span 20 facilitates the steady formation of droplets and prevents their coalescence. The viscosity of the fluid was measured by Ubbelohde viscometer (iVisc, LAUDA, Germany). The density of the fluid was measured by a vibrating tuber density meter (Anton Paar DMA-4500-M, Austria). The interfacial tension between the two phases was measured by a tensiometer (OCAH200, Data Physics instruments GmbH, Germany) via pendant drop method. The properties of liquids are shown in Table 1.

Fig. 2 shows the parameters for the calculation of the droplet volume. When the droplet length is less than $0.8W_c$ (W_c is the microchannel width), the droplet shape is approximately spherical. When the droplet length is greater than $0.8W_c$, the shape of the droplet is like a slug. The volume of the droplet could be divided into three

Table 1. Physical properties of liquids used in the experiment

Liquid	Density, ρ/kg·m^{-3}	Viscosity, μ/mPa·s	Interfacial tension, σ/mN·m^{-1}
4% span-20/mineral oil	852.9	22.23	--
Pure water	997.1	0.88	6.66
10% Gly	1020.5	1.13	3.42
20% Gly	1045.0	1.51	2.04
30% Gly	1070.5	2.10	1.80

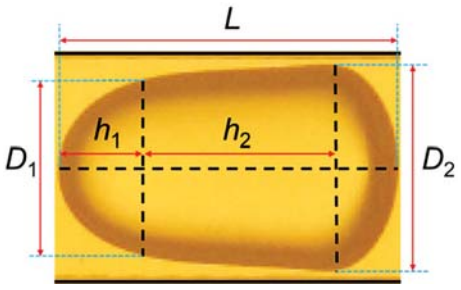

Fig. 2. Sketch of the shape of a droplet and definitions of parameters for volume calculation. L: length of droplet; height of spherical cap of the droplet head; D_1: basal diameter of spherical cap of the droplet head; h_2: height of droplet body; D_2: basal diameter of spherical cap of the droplet tail.

parts: a spherical cap for the head and tail of the droplet, and a circular truncated cone for the main part of the droplet. As the droplet length increases, the main part of the droplet turns from a circular truncated cone into a cylinder. The droplet volume is calculated as shown in Eq. (1). The accuracy of Eq. (1) was checked by comparing the volume of the mother droplet with the sum of two daughter droplets volume, and the relative error was below 5%.

$$V=\begin{cases}\frac{\pi}{6}L^3 & L\le 0.8W_c\\ \frac{1}{2}\pi h_2(D_1^2+D_2^2+D_1D_2) & \\ \quad+\frac{\pi}{8}(h_1D_1^2+(L-h_1-h_2)D_2^2) & L>0.8W_c\\ \quad+\frac{\pi}{6}(h_1^3+(L-h_1-h_2)^3) & \end{cases} \quad (1)$$

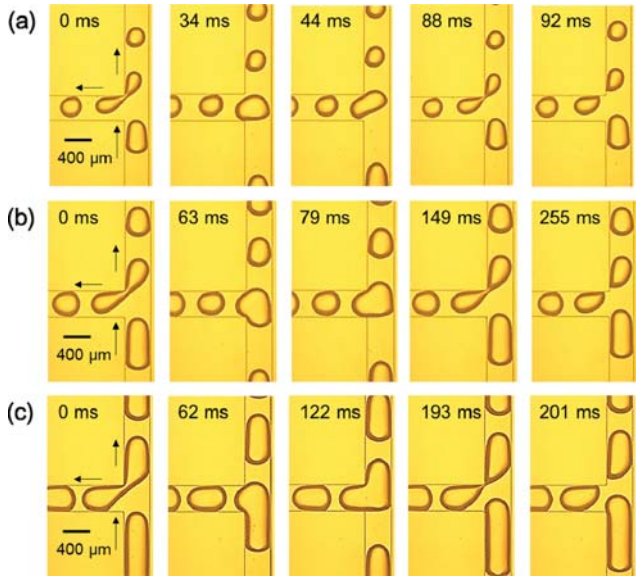

Fig. 3. Breakup process of droplet at the branching T-junction (pure water). (a) Breakup with permanent tunnel. Q_d/Q_c=0.33, Q_d= 2 ml/h; (b) breakup with part obstruction. Q_d/Q_c=1, Q_d=2 ml/h; (c) breakup with permanent obstruction. Q_d/Q_c=1.5, Q_d= 3 ml/h.

RESULTS AND DISCUSSION

1. Breakup Process of Droplet at the Branching T-junction

The breakup process of droplet at the branching T-junction is displayed in Fig. 3. The time 0 of breakup was taken as the moment when the head of the mother droplet just entered into the T-junction. As shown in Fig. 3, the deformation of the mother droplet started after time 0, and the droplet head moved forward in the axial direction and expanded in the radial direction until it contacted with the sharp corner of the T-junction. At this moment, the length of droplet head in downstream branch microchannel was longer than that in downstream main microchannel due to the asymmetry of the T-junction. As the droplet moved forward, the tail of the droplet entirely entered into the T-junction (the short droplet has entirely entered into the T-junction before it contacted with the sharp corner). Then, the neck of droplet became thinner gradually until two daughter droplets were formed. There are three flow patterns of droplets: breakup with permanent tunnel, breakup with part obstruction and breakup with permanent obstruction as shown in Fig. 3. From (Fig. 3(a)) the short droplet cannot obstruct the downstream channels during the breakup process. This type of flow pattern is named "breakup with permanent tunnel". The characteristic of "breakup with part obstruction" is that the visible gaps between the droplet and walls appear at a certain moment during the breakup process (Fig. 3(b)). As shown in (Fig. 3(c)) the characteristic of breakup with permanent obstruction is that the droplets contact with the downstream channels wall permanently during the breakup process. Wang et al. [19] also found these flow patterns in the experiment of bubble breakup at the branching T-junction.

2. Volume Distribution of Droplet at the Branching T-junction

To predict the relative size of daughter droplets, the ratio of daughter droplet volume in branch microchannel V_b to that in main microchannel V_m was defined as volume distribution ratio λ, and $\lambda=V_b/V_m$. In this experiment, the geometrical parameters of the two downstream channels are the same. To better understand the distribution behavior, the distribution of continuous phase at the T-junction without dispersed phase is shown in Fig. 4; the dotted line is the virtual boundary of the continuous phase [24].

2-1. Effect of Two Phase Flow Rates on Volume Distribution

Fig. 5 shows the effect of two phase flow rates on volume distri-

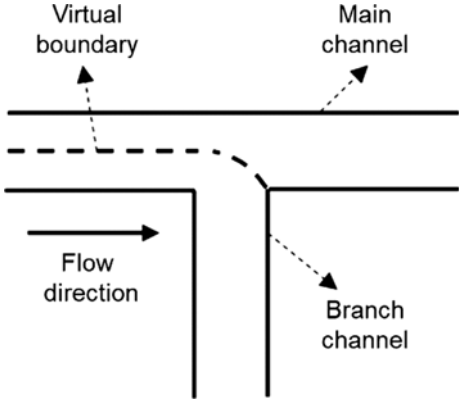

Fig. 4. Volume distribution of the continuous phase.

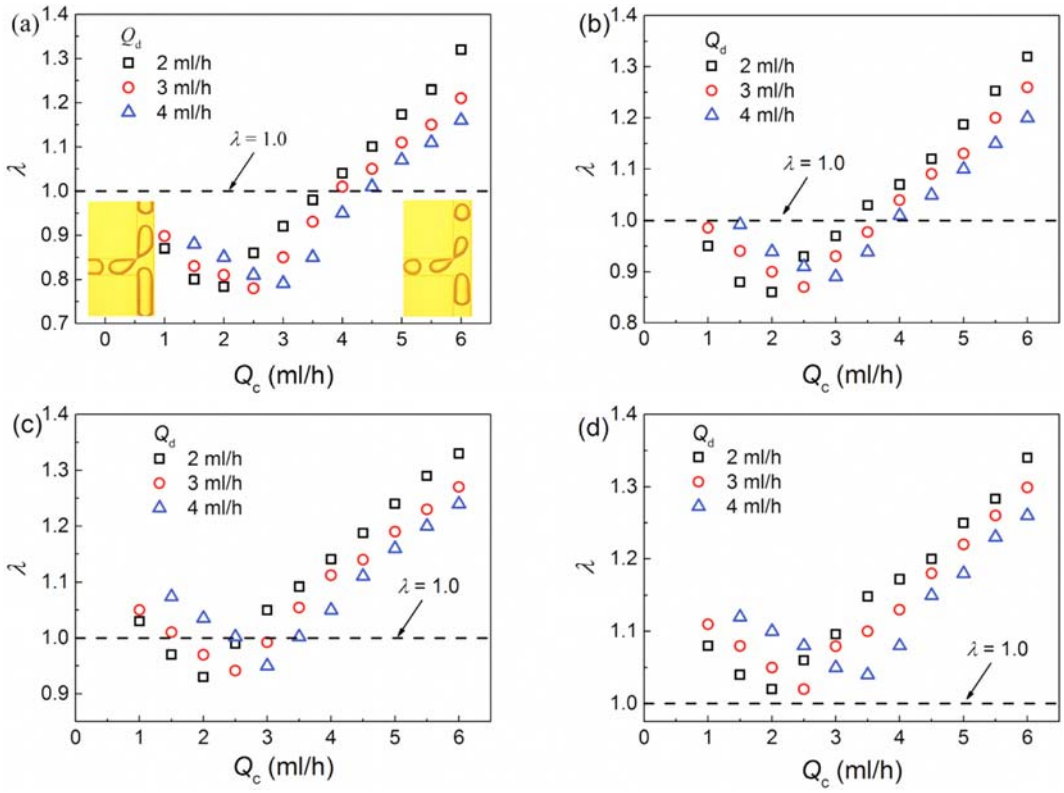

Fig. 5. Effects of two phase flow rates on volume distribution. (a) Water; (b) 10% Gly; (c) 20% Gly; (d) 30% Gly.

bution ratio λ. As shown in Fig. 5, λ could be notably affected by the flow rates of the dispersed phase and continuous phase. When the dispersed phase flow rate is fixed, λ decreases first and then increases with increasing the continuous phase flow rate with an existence of turning point. The occurrence of the turning point could be attributed to the transition of flow pattern from breakup with part obstruction (Fig. 3(b)) to breakup with permanent obstruction (Fig. 3(c)). The effect of two phase flow rates on volume distribution is mainly because the two phase flow rates would directly influence the volume of mother droplets formed in cross-focusing device [25,26] and the inertial force of liquid.

Owing to the asymmetry of branching T-junction, the droplet head is always inclined to enter the branch channel first as shown in Fig. 3; thus the branch channel has actually shown a "superiority" for droplets from the initial stage of the breakup process. For a fixed dispersed phase flow rate, the volume of mother droplets will decrease with the increase of the flow rate of the continuous phase. Before the turning point in Fig. 5, the flow pattern of droplets is breakup with permanent obstruction, and there is no tunnel between the droplet and downstream channels. With the increase of Q_c, the volume of the mother droplet would decrease, and the inertial force of continuous would increase. In this case, the fluids in the upstream channel would more easily push the droplet into the main channel. Thus, the droplet would have more part into the main chan-

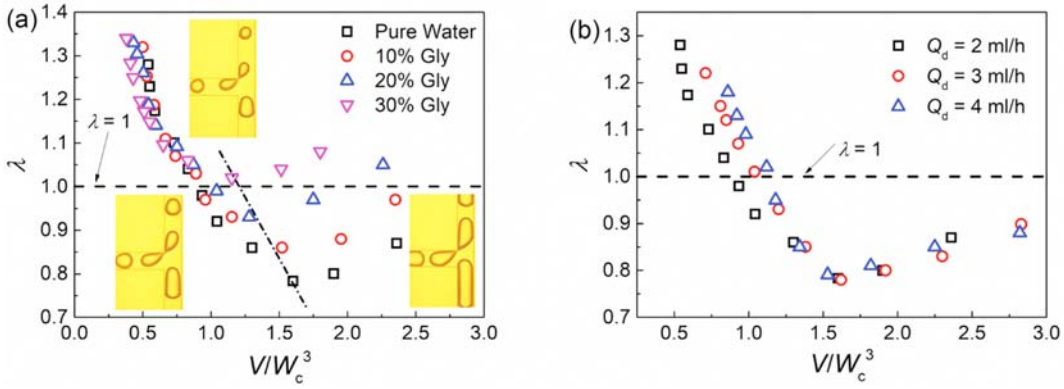

Fig. 6. Effects of the volume of the mother droplet on volume distribution. (a) Q_d=2 ml/h; (b) pure water. — · —, transition line from breakup with part obstruction to breakup with permanent obstruction.

nel; as a result, the volume distribution ratio λ decreases before the turning point. After the turning point, the flow pattern is breakup with permanent tunnel and breakup with part obstruction, as shown separately in Figs. 3(a) and (b). With the increase of Q_c, the inertial force facilitates the continuous phase more easily to remain the movement towards the main channel throw the tunnel between the droplet and channel wall, which could lead to an increase of accumulated pressure in the main channel. In this case, the pressure at the inlet of downstream main channel would increase. In addition, with the increase of continuous phase flow rate Q_c, the volume of the mother droplet would decrease, and the influence of the superiority of the branch channel would become gradually increased. Thus, the droplet would have more part into the branch channel; consequently, the volume distribution ratio λ would increase with the increase of Q_c after the turning point.

Fig. 6 shows the effect of dimensionless mother droplet volume V/W_c^3 on volume distribution ratio λ, where V is the volume of mother droplet. Similar to Fig. 5, there exist also turning points in Fig. 6. This could be attributed to the transition of flow pattern from breakup with part obstruction to breakup with permanent obstruction. Before the turning point, the flow pattern is breakup with permanent tunnel and breakup with part obstruction; as shown separately in Figs. 3(a) and (b), the shear force and inertial force held a dominant role in the breakup process of droplet [17], leading to the decline of λ with V/W_c^3. After the turning point, the flow pattern is breakup with permanent obstruction (Fig. 3(c)); the accumulated pressure in the liquid near the droplet rear predominates the breakup process of droplets, [20] resulting in the rise of λ with V/W_c^3. As shown in Fig. 6(a), when V/W_c^3 is less than 1, the distribution ratio is hardly affected by the dispersed phase. However, when the volume of the mother droplet is comparatively large, the distribution ratio is obviously affected by the dispersed phase. With the decrease of viscosity of dispersed phase, the droplet is more propitious to be pushed by upstream liquids into the main channel; thus, the λ decreases. The transition between breakup with part obstruction to breakup with permanent obstruction only depends on the size of the mother droplet for the same liquid-liquid system

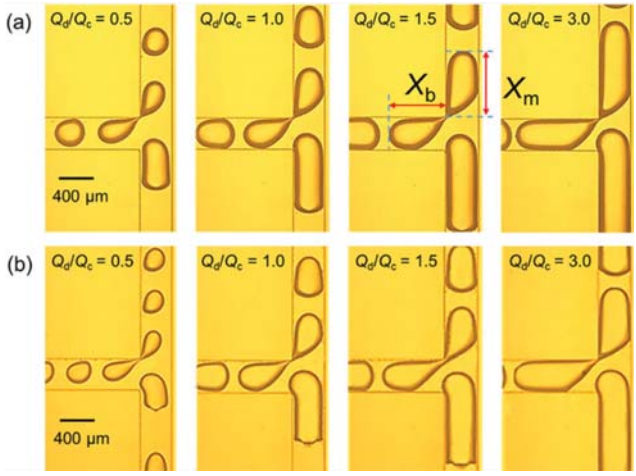

Fig. 7. Volume distribution at different flow rates of the continuous phase (Q_d=3 ml/h). (a) Water; (b) 30% Gly.

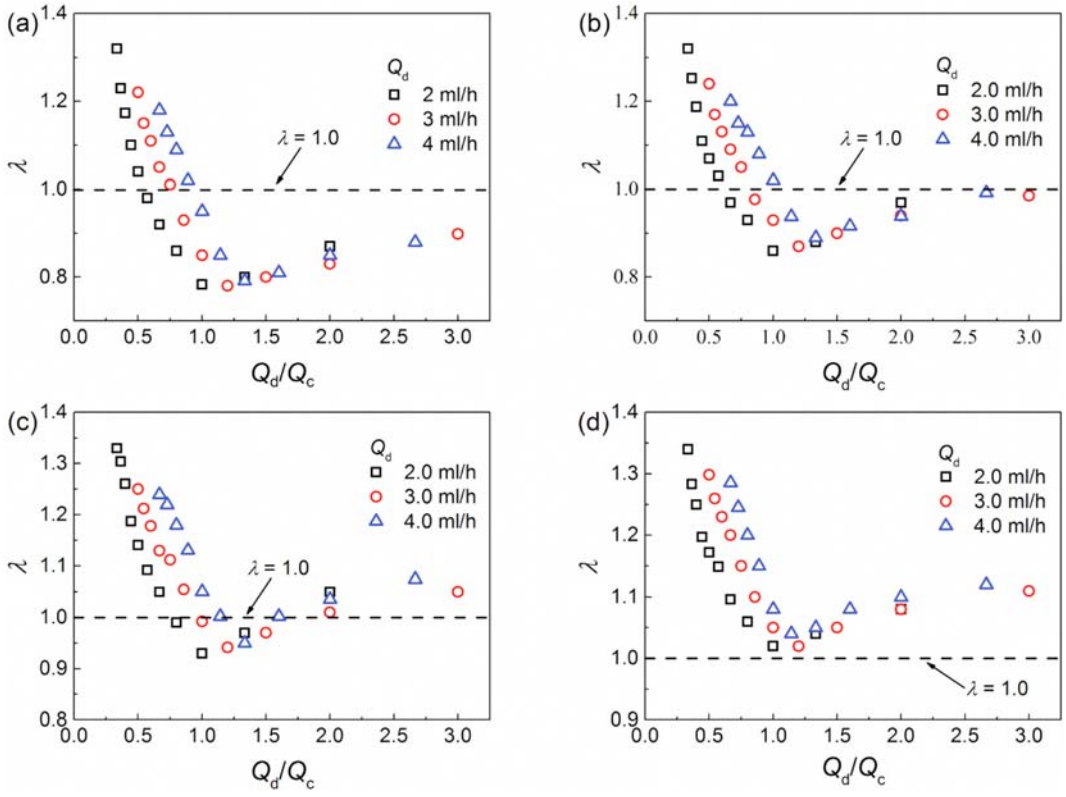

Fig. 8. Effect of flow rate ratio Q_d/Q_c on volume distribution. (a) Water; (b) 10% Gly; (c) 20% Gly; (d) 30% Gly.

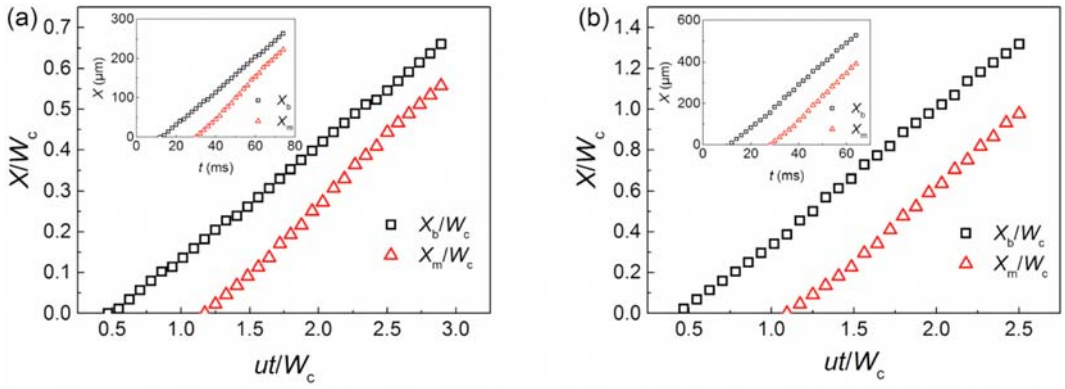

Fig. 9. Evolution of dimensionless length X_b/W_c, X_m/W_c for short mother droplet in branch channel and main channel with dimensionless time ut/W_c, (Q_d=3 ml/h, Q_c=6 ml/h). The inset shows the variation of length for mother droplet in branch channel and main channel X_b, X_m with time t. (a) Water; (b) 30% Gly.

[12,19]; correspondingly, the volumes of mother droplet at the turning point are the same when the dispersed phase is fixed (Fig. 6(b)). While, the volume of mother droplet at the turning point decreases as the viscosity of the dispersed phase increases due to the influence of the viscosity ratio between two phases on the transition of flow pattern [12] (Fig. 6(a)).

Taking the dispersed phase of pure water and 30 wt% glycerol-water solution as examples, Fig. 7 shows the distribution of mother droplets at different continuous phase flow rates when the dispersed phase flow rate is 3 ml/h. As seen in Fig. 5 and Fig. 7, the physical properties of mother droplet have nonnegligible influence on the volume distribution. As shown in Table 1, the changes of glycerol mass concentration lead to the differences of the viscosity and interfacial tension of the aqueous solutions. Under the combined effects of the interfacial tension and the viscosity of dispersed phase, the minimum value of volume distribution ratio λ would increase with the increase of glycerol mass concentrations in glycerol-water solution.

Fig. 8 shows the effect of flow rate ratio Q_d/Q_c on volume distribution ratio λ. As shown in Fig. 8, the volume distribution ratio λ decreases at first and then increases with the increase of Q_d/Q_c, with a turning point around Q_d/Q_c=1.25.

The volume distribution of mother droplets with similar size depends on the physical properties. This is mainly due to the difference in the movement velocity of droplet head in the downstream branch channel and main channel. To fully understand the volume distribution of droplet breakup into two daughter droplets, the evolution of droplet head in downstream channels was also studied. As shown in Fig. 7(a), the droplet lengths in the downstream branch and main channels are marked as X_b and X_m, respectively. X_b and X_m are further normalized by the channel width W_c, and the time t is normalized by W_c/u, where u ($u=(Q_c+Q_d)/W_c^2$) is the superficial velocity of fluids. Fig. 9 shows the evolution of short droplet X_b/W_c and X_m/W_c with ut/W_c in the whole breakup process: from entering the T-junction to break up into two daughter droplets. As seen in Fig. 9, the evolution of X_b/W_c and X_m/W_c over dimensionless time ut/W_c is not strictly linear. During the droplet breakup process, the short droplet cannot completely obstruct the downstream channels; the droplet breakup process is affected by both shearing force and accumulated pressure of continuous phase. In different stages of the breakup process, the roles of these two forces are different; consequently, the trend of droplet head evolution is not a straight line [27]. As shown in Fig. 9, for short droplet the length in the main channel is always less than that in the

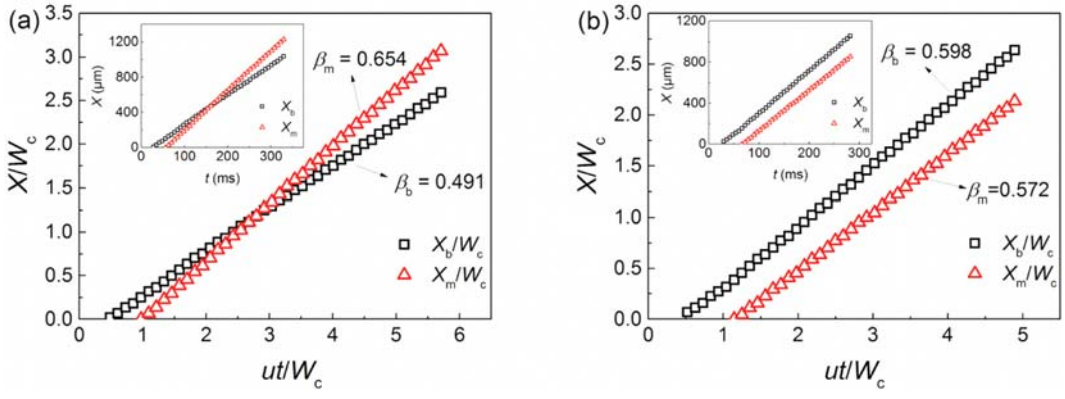

Fig. 10. Evolution of dimensionless length X_b/W_c, X_m/W_c for long mother droplet in branch channel and main channel with dimensionless time ut/W_c, (Q_d=3 ml/h, Q_c=1 ml/h). The inset shows the variation of length for mother droplet in branch channel and main channel X_b, X_m with time t. (a) Water; (b) 30% Gly.

branch channel during the whole breakup process; as a result, the volume distribution ratio would be greater than 1. As shown in Fig. 7, with the decrease of Q_d/Q_c, the mother droplet volume decreases. As the mother droplet volume decreases, the final breakup dimensionless time uT/W_c is shortened, where T is the period from the droplet entering the T-junction to final breakup, and the size difference between two daughter droplets becomes greater. Consequently, the volume distribution ratio λ increases with the decrease of Q_d/Q_c for short droplets. Wang et al. [19] found that when the continuous phase flow rate is high, short bubbles always enter into the branch channel due to the effect of the flow field of continuous phase. This is an extreme situation; in this case, the volume distribution ratio λ is towards infinitely great.

Fig. 10 shows the evolution of the X_b/W_c and X_m/W_c with ut/W_c for long droplet. As seen in Fig. 10, both X_b/W_c and X_m/W_c vary linearly with dimensionless time ut/W_c. The variation rates are marked as β_b and β_m. A similar phenomenon was also reported for the droplet breakup at symmetric T-junctions [12]. Jullien et al. [12] found that the position of droplet head in branch channel varied linearly with dimensionless time, due to the accumulated pressure in the liquid near the droplet rear. As shown in Fig. 10, the length of droplets in the branch channel will catch up with and surpass the length of droplets in the main channel when the dispersed phase is pure water, thereby resulting in a volume distribution ratio less than 1. However, as the variation rate β_b is slightly larger than β_m and the mother droplet will always enter the branch channel first, hence the length of droplet in main channel is always less than that in the branch channel for 30 wt% glycerol-water solution, and the volume distribution ratio is greater than 1.

2-2. Effect of Two Phase Reynolds Numbers on Volume Distribution

Logically, the droplet breakup stems from various forces, which leads to different volume distributions of droplets. The changes of the forces rely mainly on the flow rate and physical property of liquid-liquid two-phase system. Fig. 11 shows the effect of two-phase Reynolds number (the relative importance of inertial force to viscous force) on volume distribution ratio λ. The Reynolds number of the continuous phase can be defined as $Re_c=W_c u_c \rho_c/\mu_c$, where u_c ($u_c=Q_c/W_c^2$) is the superficial velocity of continuous phase, ρ_c is the density of continuous phase, and μ_c is the viscosity of continuous phase. The Reynolds number of the dispersed phase can be defined as $Re_d=W_c u_d \rho_d/\mu_d$, where u_d ($u_d=Q_d/W_c^2$) is the superficial velocity of dispersed phase, ρ_d is the density of dispersed phase, and μ_d is the viscosity of dispersed phase. Similar to Fig. 5, the volume distribution ratio λ decreases at first and then increases with the increase of the continuous phase Reynolds number Re_c when the dispersed phase Reynolds number Re_d is fixed. When continuous phase Reynolds number Re_c is fixed, the changes of Reynolds number Re_d depend mainly on the physical property of dispersed phase. The volume distribution ratio λ decreases with the increase of the dispersed phase Reynolds number Re_d. With the increase of Re_d, the effect of dispersed phase inertial force on volume distribution becomes gradually increased. The mother droplet more easily keeps the moving trend towards the main channel, which could lead to an increase of the volume of daughter droplet in the main channel.

2-3. Effect of Dispersed Phase Capillary Number on Volume Distribution

Fig. 12 shows the effect of capillary number of the dispersed phase (the relative importance of viscous force to interfacial tension) on volume distribution ratio λ. The capillary number of the dispersed phase is defined as $Ca_d=\mu_d u_d/\sigma$, where σ is the interfacial tension of two phase. As shown in Fig. 12, when the flow rate ratio is fixed, the volume distribution ratio λ increases with the increase of dispersed phase capillary number Ca_d. For different flow rate ratios, the variation trends of λ with dispersed phase capillary number Ca_d are similar. In the present work, the $Ca_{d,max}=0.0081$, indicating that the effect of viscous of the dispersed phase on the breakup process is weaker in comparison with the interfacial tension. The mother droplet could block the branch channel during the droplet breakup process. Under the small Ca_d situation, the mother droplet does not easily deform due to high interfacial tension; thus, the block effect is more remarkable with a small λ. However, with the increase of Ca_d, the block effect of mother droplet on branch channel becomes weakened, accordingly leading to a large λ. Chen et al. [22] also found that the block effect of mother

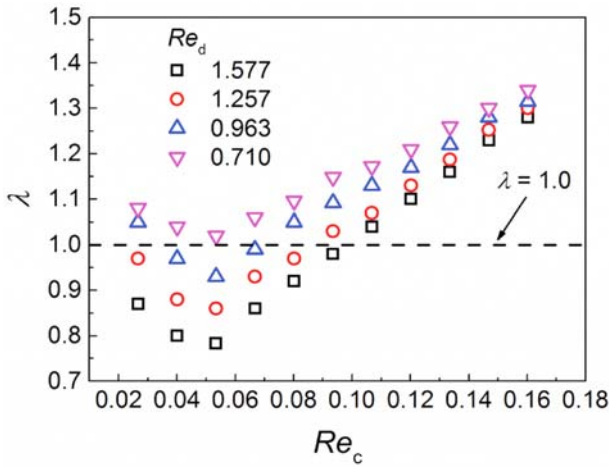

Fig. 11. Effect of Reynolds number on volume distribution (Q_d=2 ml/h).

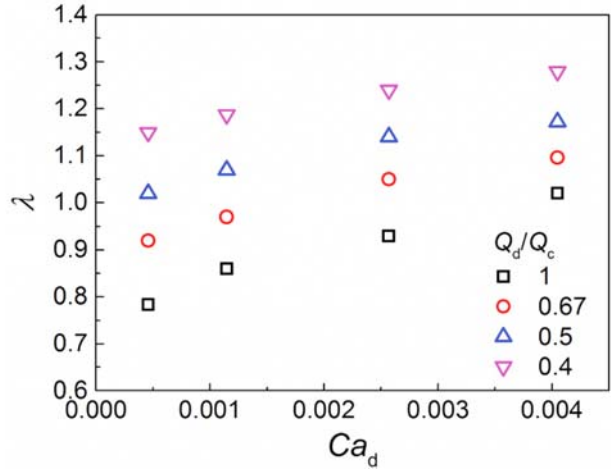

Fig. 12. Effect of capillary number of the dispersed phase on volume distribution (Q_d=2 ml/h).

bubble on branch channel relies dramatically on the interfacial tension.

3. Prediction Model of Droplet Volume Distribution

In recent years, several efforts have been devoted to the prediction of droplet (bubble) volume distribution at T-junctions. When the lengths of the two downstream channels are different, Link et al. [7] analogized the microfluidic device with an electric-current-splitting device. They found $\lambda=V_b/V_m\approx l_m/l_b$ (l_m and l_b are the length of downstream branch channel and main channel, respectively). However, the analogy of the microfluidic device with an electric-current-splitting device has some limitations. For example, not all droplets reaching the T-junction break up. In addition, unlike electric-current-splitting device, both the dispersed phase and the continuous phase flow in the microchannel simultaneously. Therefore, an analysis aimed only at the droplet (bubble) is inaccurate. When the cross-section of the two downstream channels is different, Bedram et al. [16] and Samie et al. [17] found that the relationship between volume ratio of two daughter droplets with the two downstream channels width ratio shows a power law: $\lambda=V_b/V_m\propto(W_{c,b}/W_{c,m})^{\alpha}$ (α is an experimental fitting parameter).

To accurately predict the distribution of droplets at branching T-junction, the volume distribution ratio λ was fitted by the following dimensionless parameters: the flow rate ratio Q_d/Q_c, the dispersed phase capillary number Ca_d, the continuous phase Reynolds numbers Re_c and the dispersed phase Reynolds number Re_d. Dividing by the value of Re_c at the turning point in Fig. 11, the experimental data were fitted:

$$\lambda=\begin{cases}1.64(Q_d/Q_c)^{0.042}Ca_d^{0.094}Re_c^{-0.024}Re_d^{-0.045} & Re_c\le 0.053\\ 2.13(Q_d/Q_c)^{-0.138}Ca_d^{0.018}Re_c^{0.258}Re_d^{-0.087} & Re_c>0.053\end{cases} \quad (2)$$

As seen in Eq. (2), when $Re_c\le 0.053$, the volume distribution ratio λ increases with the increase of Q_d/Q_c and the decease of Re_c. However, the opposite trend can be found when $Re_c>0.053$. The variation trend of λ shows good agreement with the phenomena displayed in Fig. 8 and Fig. 11. Moreover, the volume distribution ratio λ always decreases with the increase of Re_d and the decrease of Ca_d, which shows good agreement with the phenomena displayed in Fig. 11 and Fig. 12. Fig. 13 shows the comparison between predicted values and experimental data of volume distribution ratio, with the average relative error of 4.16% and the maximum relative error of 12.52%. The results show that the model can precisely predict the volume distribution ratio of droplets at the branching T-junction.

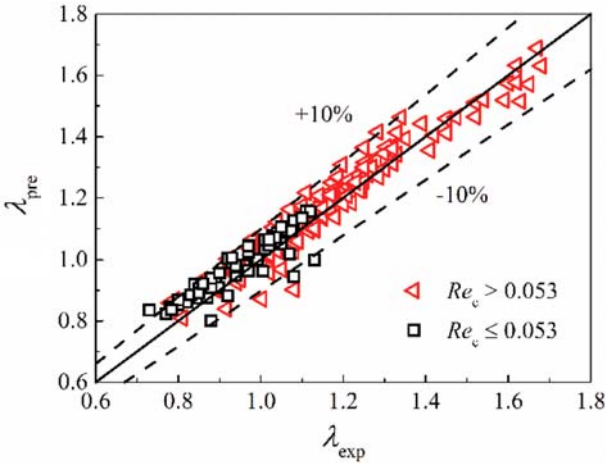

Fig. 13. Comparison between predicted values and experimental data of volume distribution ratio.

CONCLUSIONS

The manipulation mechanism of droplet volume distribution at branching T-junction was highlighted. For a fixed flow rate of the dispersed phase, the volume distribution ratio λ decreases first and then increases with the increase of the two-phase flow rate ratio Q_d/Q_c. For a given Reynolds number Re_d of the dispersed phase, the volume distribution ratio λ decreases first and then increases with the increase of the Reynolds number Re_c of the continuous phase. For a constant Reynolds number Re_c of the continuous phase, the volume distribution ratio λ decreases with the increase of the Reynolds number Re_d of the dispersed phase. When the two-phase flow rate ratio Q_d/Q_c is fixed, the larger the capillary number Ca_d of the dispersed phase is, the larger is the volume distribution ratio λ. To predict the droplet volume distribution ratio accurately, predictive correlations were proposed. The results in this work could provide guidance for the design and application of a multi-branch microchannel device.

ACKNOWLEDGEMENT

The work was supported by the National Nature Science Foundation of China (No. 21776200, 21576186, 91634105, 91434204), and the aid of Opening Project of State Key Laboratory of Chemical Engineering (No. SKL-ChE-17B02).

NOMENCLATURE

Ca : capillary number
D_1 : basal diameter of spherical cap of droplet head [m]
D_2 : basal diameter of spherical cap of droplet tail [m]
h_1 : height of spherical cap of droplet head [m]
h_2 : height of droplet body [m]
l : length of microchannel [m]
L : length of droplet [m]
Q : volumetric flow rate [$m^3\cdot s^{-1}$]
Re : Reynolds number
X : distance between the droplet and the T junction [m]
t : time [s]
T : droplet breakup period [s]
u : superficial velocity of liquid [$m\cdot s^{-1}$]
W_c : width of the channel [m]
We : Weber number
α : experimental fitting parameter
β : slope of a line
ρ : density of liquid [$kg\cdot m^{-3}$]
μ : viscosity of liquid [Pa·s]

σ : interfacial tension of liquid [$N \cdot m^{-1}$]
λ : volume distribution ratio

Subscripts
b : branch channel
c : continuous phase
d : dispersed phase
m : main channel

REFERENCES

1. H. Song, J. D. Tice and R. F. Ismagilov, *Angew. Chem.*, **115**, 792 (2003).
2. S. K. Min, B. M. Lee, H. H. Jin, S. H. Ha and H. S. Shin, *Korean J. Chem. Eng.*, **29**, 392 (2012).
3. J. Santos, L. A. Trujillo-Cayado, N. Calero, M. C. Alfaro and J. Muñoz, *J. Ind. Eng Chem.*, **36**, 90 (2016).
4. R. S. Boogar, R. Gheshlaghi and M. A. Mahdavi, *Korean J. Chem. Eng.*, **30**, 45 (2013).
5. J. W. Hwang, J. H. Choi, B. Choi, G. Lee, S. W. Lee, Y. M. Koo and W. J. Chang, *Korean J. Chem. Eng.*, **33**, 57 (2016).
6. T. Cubaud and C. M. Ho, *Phys. Fluids*, **16**, 4575 (2004).
7. D. R. Link, S. L. Anna, D. A. Weitz and H. A. Stone, *Phys. Rev. Lett.*, **92**, 054503 (2004).
8. A. M. Leshansky and L. M. Pismen, *Phys. Fluids*, **21**, 023303 (2009).
9. M. Belloul, W. Engl, A. Colin, P. Panizza and A. Ajdari, *Phys. Rev. Lett.*, **102**, 194502 (2009).
10. P. Parthiban and S. A. Khan, *Lab Chip*, **12**, 582 (2012).
11. B. M. Jose and T. Cubaud, *Microfluid. Nanofluid.*, **12**, 687 (2012).
12. M. C. Jullien, M. J. Tsang Mui Ching, C. Cohen, L. Menetrier and P. Tabeling, *Phys. Fluids*, **21**, 072001 (2009).
13. D. A. Hoang, L. M. Portela, C. R. Kleijn, M. T. Kreutzer and V. van Steijn, *J. Fluid Mech.*, **717** (2013).
14. B. Chen, G. Li, W. Wang and P. Wang, *Appl. Therm. Eng.*, **88**, 94 (2015).
15. Y. Yong, S. Li, C. Yang and X. Yin, *Chin. J. Chem. Eng.*, **21**, 463 (2013).
16. A. Bedram and A. Moosavi, *Eur. Phys. J. E*, **34**, 78 (2011).
17. M. Samie, A. Salari and M. B. Shafii, *Phys. Rev. E: Stat. Nonlinear Soft Matter Phys.*, **87**, 053003 (2013).
18. T. Fu, Y. Ma and H. Z. Li, *AIChE J.*, **60**, 1920 (2014).
19. X. Wang, C. Zhu, T. Fu and Y. Ma, *Chem. Eng. Sci.*, **111**, 244 (2014).
20. X. Wang, C. Zhu, T. Fu and Y. Ma, *AIChE J.*, **61**, 1081 (2015).
21. T. Moritani, M. Yamada and M. Seki, *Microfluid. Nanofluid.*, **11**, 601 (2011).
22. J. Chen, S. Wang and S. Cheng, *Chem. Eng. Sci.*, **84**, 706 (2012).
23. Y. Liu, W. Sun and S. Wang, *Chem. Eng. Sci.*, **158**, 267 (2017).
24. J. Kim, J. Won and S. Song, *Biomicrofluidics*, **8**, 054105 (2014).
25. S. Lignel, A. V. Salsac, A. Drelich, E. Leclerc and I. Pezron, *Colloids Surf. A*, **531**, 164 (2017).
26. W. Du, T. Fu, C. Zhu, Y. Ma and H. Z. Li, *AIChE J.*, **62**, 325 (2016).
27. T. Fu, Y. Ma, D. Funfschilling and H. Z. Li, *Chem. Eng. Sci.*, **66**, 4184 (2011).